

# RXTE highlights of 34.85-day cycle of Her X-1

N.I.Shakura<sup>1</sup>, N.A.Ketsaris<sup>1</sup>, M.E.Prokhorov<sup>1</sup> and K.A.Postnov<sup>2</sup>

<sup>1</sup> *Sternberg Astronomical Institute, 119899 Moscow, Russia*

<sup>2</sup> *Faculty of Physics, Moscow State University, 119899 Moscow, Russia*

Accepted 1998... Received 1998 ...

## ABSTRACT

An analysis of the publically available RXTE archive on Her X-1 including data on 23 34.85-day cycles is performed. The turn-on times for these cycles are determined. The number of cycles with a duration of 20.5 orbits has been found exceedingly larger than of shorter (20 orbits) or longer (21 orbits). A correlation between the duration of a cycle and its mean X-ray flux is noted. The mean X-ray light curve shows a very distinct short-on state. The anomalous X-ray absorption dip is found during the first orbit after the turn-on in the main-on state for the cycles starting near the binary phase 0.25, while is present during two successive orbits in the low-on state. The post-eclipse recovery feature have not been found in the main-on state but appears at least for two orbits during the low-on state. The pre-eclipse dips are present both in main-on and low-on state and demonstrate the behaviour as in early observations. The comparison of durations of the main-on and short-on states enabled us to constrain the accretion disk semi-thickness and its inclination to the orbital plane.

**Key words:** X-ray: stars – Stars: binary – Stars: individual: Her X-1

## 1 INTRODUCTION

Her X-1 is one the first X-ray binary pulsar discovered by the eminent UHURU satellite in 1972 (Tananbaum et al. 1972, Giacconi et al. 1973) and since then remains one of the most studied accretion-driven X-ray stellar binaries. The pulsar is an accretion-powered magnetized rotating ( $P = 1.24$  s) neutron entering an eclipsing X-ray binary with a low-mass ( $\sim 2M_{\odot}$ ) optical companion in a practically circular orbit with a period of 1.7 d. The binary orbit inclination is  $i = 85 - 88^{\circ}$ , the total duration of the X-ray eclipse is around 20,000 s. The optical counterpart, HZ Her, first suggested by Liller (1972), provides a classical example of the reflection effect when the strong orbital modulation in optics is due to a powerful illumination of the part of normal star atmosphere facing X-ray source (Bahcall & Bahcall 1972; Cherepashchuk et al. 1972). The amplitude of the reflection effect strongly increases in ultraviolet and according to many optical UB<sub>V</sub>-photometrical data is  $\Delta m_V = 1.45$ ,  $\Delta m_B = 1.6$ ,  $\Delta m_U = 2.55$ .

Already very first UHURU observations of Her X-1 revealed the presence of a long-term 34.85-d cycle. Its properties have been so interesting that practically all specialized X-ray satellites studied it (among which Copernicus, Ariel-5, Ariel-6 (Davison & Fabian 1974, 1977, Ricketts et al. 1982), HEAO-1 (Gorecki et al. 1982, Soong et al. 1987), Hakucho and TENMA (Nagase et al. 1984, Ohashi et al. 1984), EXOSAT (Ögelman & Trümper

1988), Ginga (Deeter et al. 1991), Astron (Sheffer et al. 1992), BATSE (Wilson et al. 1994), and RXTE (see [http://space.mit.edu/XTE/asmlc/srcs/data/herx1\\_105.dat](http://space.mit.edu/XTE/asmlc/srcs/data/herx1_105.dat))). RXTE data are shown in Fig. 1.

The gross shape of the X-ray light curve consists of a main-on X-ray state with a mean duration of 7 orbital periods surrounded by two off-states each 4 orbital cycles in duration, and of a secondary short-on state of smaller intensity with a typical duration of  $\sim 5.5$  orbital cycles. The form of the X-ray light curve is asymmetric: in the main-on state the X-ray intensity rapidly increases during 1.5–2 orbital cycles, stays at maximum over 2.5 cycles, and then decreases to a minimum in the successive 3 orbital revolutions. At the beginning of the ascending branch a strong low-energetic absorption dominates in the X-ray spectrum while at the descending part it does not vary appreciably. A characteristic feature of the X-ray light curve is the presence of strong pre-eclipse and anomalous absorption dips during the main-on state. The anomalous dips are generally found only in the first or second orbit after turn-on near orbital phase 0.55. The pre-eclipse dips march from the eclipse toward earlier orbital phase in successive orbits. Sometimes, a post-eclipse recovery is observed in the second orbit after turn-on.

The short-on X-ray state was found with the Copernicus satellite (Fabian et al. 1973) and later observed with Ariel-5 (Cooke & Page 1975). Subsequently, Jones & Forman (1976) found the short-on state in the UHURU records.

Most observed details of the X-ray light curve can be naturally explained by the model of tilted accretion disk undergoing the counter-precession opposite to the orbital motion (Gerend & Boynton 1976, Crosa & Boynton 1980). At the main-on state, the disk is mostly opened to the observer (the total inclination angle represents a combination of the binary and disk inclinations), at the low-on state the opening angle is smaller. The X-ray source turn-off seen for a few orbits is due to the screening by the thick accretion disk. In fact, a weak X-ray glow is observed during the off-states, which is apparently due to scattering on the electrons of an extended accretion disk corona (Jones & Forman 1976).

As was discovered by UHURU and confirmed by the subsequent observations, the main turn-on times preferentially occur around 0.25 and 0.75 orbital phases of the binary system. Levine & Jernigan (1982) suggested that this tendency is due to nutation effects of an inclined precessing accretion disk.

Staubert et al. (1983) analysed turn-on data and concluded that the actual separation between two successive turn-ons may be either 20.0, 20.5 or 21.0 binary cycles selected random with equal statistical probabilities. Baykal et al. (1993) revealed that the statistical interpretation of turn-on behaviour is consistent with a white-noise process in the first derivative of the 35-d phase fluctuations (or a random walk in clock phase). It remains unclear up to now why the precessional period is so close to 20.5 orbital cycles ( $1.7 \times 20.5 = 34.85$  days!).

The traces of 34.85-d cycle have also been found in optical modulation of HZ Her (Kurochkin 1972). Gerend & Boynton (1976) modeled the optical light curve by thick precessing tilted accretion disk. Afterwards, Howarth & Wilson (1983), using more extended photometrical data, came to similar conclusions.

Variability of the source on longer time scales is also very surprising. In 1983, the EXOSAT observations detected a 9-months' turn-off of the X-ray source (IAUC 3852, 1983) during which the reflection effect was however persistent in optics (Mironov et al. 1984). Notably, the subsequent normal turn-on of the X-ray source occurred practically in phase with the mean ephemeris calculated for 20.5 orbital cycles periodicity (Ögelman et al. 1985) and since then the source have not shown visible deviations from the mean schedule.

A few episodes of significant decrease of the optical reflection effect and fading of HZ Her have been found in Zonnenberg archive optical plates (Wentzel & Gessner 1972). Jones et al. (1973) analysed almost 100-years' Harward phototeque and found also several episodes of the absence of the reflection effect with a duration from ten days to years. During such off-states the light curve of HZ Her decreased in amplitude down to  $\sim 0.^m3$ , had a double-wave shape, and was solely due to ellipsoidal form of HZ Her.

In spite of the wealth of X-ray and optical data, the nature of the 34.85-d cycle in Her X-1 still remains controversial. In addition to the model of precessing accretion disk, a free precessing neutron star was suggested to underly 34.85-d clock mechanism (Brecher 1972, Shklovskii 1973, Novikov 1973, etc.). The evidence of the free precessing neutron star was found in EXOSAT observations (Trümper et al. 1986). Recently, to explain the rapid change of X-ray pulse form during the main-on state observed by HEAO-1 in 1978, we

suggested a model of free precessing triaxial neutron star (Shakura et al. 1998).

With the launch of all-sky X-ray monitors (ASM) onboard Compton Gamma-Ray Observatory (CGRO) (experiment BATSE) and Rossi X-ray Time Explorer (RXTE) satellites, the new possibility emerged of collecting continuous X-ray data and thereby of studying long-term X-ray behaviour of Her X-1. This advantage of BATSE observations has been used by Wilson et. al (1994) to reveal a significant (but not universal, see a detailed review by Bildsten et al. 1997) correlation between the X-ray pulsar frequency derivative  $\dot{\nu}$  and X-ray flux at the peak of the main-on portion of 34.85-d cycle, and to confirm a possible correlation of early turn-ons with decreased mass transfer rate suggested by Ögelman (1987).

The purpose of this paper is to analyse properties of 34.85-d X-ray cycle of Her X-1 using publically available RXTE data.

## 2 THE DATA AND ANALYSIS

### 2.1 Turn-on time determination

RXTE data archive contains X-ray (2-12 keV) count rates averaged over predominantly 90-s time intervals (Fig. 1) started from MJD 50087. New data is added daily to the archive. Despite some gaps in the data, the archive is especially useful in reconstructing the mean X-ray light curve by means of superposing many cycles with account of turn-on times phases. In addition, it is possible to determine the turn-on times of 35-day cycle with a good accuracy.

This accuracy is limited by the RXTE observations (the maximum UHURU count rate from Her X-1 was about 100 counts per second while that of RXTE is about  $\leq 10$  counts per second);, nevertheless, for cycles with no gaps in data, one may clearly distinguish around which orbital phase, 0.25 or 0.75, each cycle was turned-on (see Table 1).

To construct the mean X-ray light curve of Her X-1, we first determined turn-on times. Using the ephemeris of X-ray eclipse

$$t_{min} = JD2441329.57519 + 1^d.70016773 \times E$$

as given by Deeter et al. (1981) <sup>\*</sup>, we reduced all data to the Solar system barycenter.

For well-filled cycles, we have inspected the binary phase intervals about  $\sim 0.25$  and  $\sim 0.75$  preceding the X-ray source turn-on. For this purpose, we have combined consecutive data counts into groups such that the time interval between each two adjacent points inside a group does not exceed 0.01 JD. The group has been centered to the mean time of the points inside it.

The observed count rates,  $C_i$ , were averaged inside these groups with a weight inversely proportional to variance  $\sigma_i^2$

$$\langle S \rangle = \frac{\sum_{i=1}^n \frac{C_i}{\sigma_i^2}}{\sum_{i=1}^n \frac{1}{\sigma_i^2}},$$

<sup>\*</sup> A slight decrease in orbital period of Her X-1 discovered by Deeter et al. (1991)  $\dot{P}_b/P_b = (-1.32 \pm 0.16) \times 10^{-8} \text{ yr}^{-1}$  has no effect on our results.

This figure is available at URLs:

<http://xray.sai.msu.ru/pub/preprints/Prokhorov/rxte/fig1.ps>  
 or  
<http://xray.sai.msu.ru/pub/preprints/Prokhorov/rxte/fig1.ps>

**Figure 1.** RXTE light curve of Her X-1 in counts per second as a function of MJD. Error bars (in the bottom right corner) show minimal, mean, and maximal 1- $\sigma$  errors of individual points.

**Table 1.** Turn-on time determination data

No	state	MJD	$\Phi_b$	$\Delta$	Tmpl[ $\Phi_b$ ]		Tmpl[ $\Phi_b - 0.5$ ]		Tmpl[ $\Phi_b + 0.5$ ]	
					t/u	p(%)	t/u	p(%)	t/u	p(%)
253	m	50146.565	>0.07–0.24		10/7	95	9/6	13	17/13	42
				20.5	18/11	93				
254	m	50181.419	0.65–0.73		7/5	90	12/8	13		0
				20.5	18/14	86				
255	m	50216.272	0.22–0.34		10/7	78		0	18/14	95
				20.5						
256	m	50251.126	~0.75		18/15	78		0		0
				20.5						
257	m	50285.979	0.21–0.24		10/7	77		0	10/7	18
				20.5						
258	m	50320.833	~0.75		9/6	99	10/7	11		0
				20.5						
259	m	50355.686	~0.25		6/5	52	7/5	7		0
				20.5	18/10	52				
260	m	50390.540	0.69–0.72		13/10	83		0		0
				20.5						
261	h	50425.393	0.21–0.25		12/9	99		0		0
				20.5						
262	h	50460.246	~0.75		18/13	99		0	10/8	24
				21.0						
263	l	50495.950	0.61–0.80		14/9	92		0		0
				20.5						
264	m	50530.803	0.20–0.40		6/5	91		0	12/9	49
				20.5	18/11	97				
265	h	50565.657	0.62–0.70		18/13	81		0		0
				20.5						
266	h	50600.510	~0.25		12/6	>99	11/6	87	18/10	5
				21.0						
267	m	50636.214	~0.25		6/5	70		0		0
				20.0	18/11	70				
268	m	50670.217	~0.25		16/5	71		0		0
				20.5						
269	h	50705.071	0.63–0.67		6/5	88		0		0
				20.5	9/7	84				
270	l	50739.924	~0.25		6/6	88	6/6	34		0
				20.0	14/11	85				
271	l	50773.927	>0.07–0.31		18/8	76		0		0
				20.0						
272	l	50807.931	~0.25		17/12	72	7/5	33		0
				20.5						
273	m	50842.784	>0.5–0.74		7/5	77		0		0
				20.5	18/14	80				
274	m	50877.639	0.27–0.39		6/6	78		0		0
				20.5	10/8	77				
275	l	50912.492	0.63–0.71		13/10	99		0		0
				>20	18/15	>99				

where  $n$  is the total number of individual points in each group. After that we determined the total variance in each group as

$$D^2 = \frac{1}{n} \sum_{i=1}^n \sigma_i^2 + \frac{n}{n-1} \frac{\sum_{i=1}^n \frac{((S)-C_i)^2}{\sigma_i^2}}{\sum_{i=1}^n \frac{1}{\sigma_i^2}}$$

Next we have compared the signal-to-noise ratio

$$\frac{S}{N} = \langle S \rangle \frac{\sqrt{n}}{D}$$

of the neighbour groups until a group with  $S/N \gtrsim 3\sigma$  has been found. The turn-on time has been considered to lie between this groups (see Table 1). This methodics has enabled us to determine the turn-on times for 14 cycles with a typical accuracy of  $\Delta\Phi_b \sim 0.05 - 0.08$ . Due to gaps in data, for 3 cycles (## 259, 262, 270) the turn-on times have been to a half-orbit accuracy, and for remaining 6 cycles the data gaps are so large that the accuracy of the turn-on time determination is more than one orbital period.

To recover the turn-on times of 9 cycles with data gaps, using 14 well-defined cycles, we have constructed templates, separately for cycles turned-on at  $\Phi_b = 0.25$  and  $0.75$ , by averaging all "0.25-cycles" and "0.75-cycles" inside 0.068-0.5 and 0.5-0.932 orbital phase intervals (excluding X-ray eclipses). Of course, actual turn-on phase of a, say, "0.25-cycle" differs from 0.25, but when averaging no phase shifts were made for different cycles.

Since the mean X-ray amplitude of the cycles varies, no unique template can be constructed. So we have categorized all cycles into three X-ray intensity groups (high, medium, low; see Table 1) and have constructed templates for each group separately. Cycles # 263 and # 275 can be classified as "conditionally low" since they are morphologically different from all other cycles, high, low, and medium: their intensity reaches maximum during 3 orbits while all others during 1-1.5 orbital periods.

After that we have checked each template to the data-poor cycles, with the cycle data having been preliminary averaged in the same phase bins as the template points. Each trial included applying one of the 0.25-templates or 0.75-templates to the cycle checked and calculating a  $\chi^2$  test. Minimum  $\chi^2$  has been considered indicative of the most plausible template allowing the turn-on time to be recovered. First we apply this procedure to 3 cycles with 0.5-orbital phase turn-on time uncertainty, each time adding the newly categorized cycle to the template, then the procedure was repeated for remaining 6 cycles.

The template points included mainly the main-on state and few points before and after it. Note that the points near pre-eclipse X-ray absorption dips (around orbital phase 0.75) have been excluded from templates because they are strongly affected to the average X-ray intensity variations caused by data gaps around dips. For the same reason, for some cycles with data gaps preceding the turn-on, the first point with notable signal was excluded as well.

The results of turn-on times determination are collected in Table 1. The first column of Table 1 contains the standard cycle number counted from first UHURU observations. The second column shows to which intensity group, medium (m), high (h) or low (l), the cycle belongs. The third column

displays modified Julian dates ( $MJD = JD - 2,400,000.5$ ). The fourth column contains the orbital phase  $\Phi_b$  of the turn-on. The fifth column shows the cycle duration  $\Delta$  expressed in binary orbits rounded to 0.5. The sixth column shows the total number of points in the template used (t) vs. the actual number of points of this template (u) in which  $\chi^2$  test was calculated. The significance level is in the seventh column. For comparison, columns 8-9 are the same as 6-7, but for templates shifted by  $-0.5$  cycles earlier the turn-on found. Columns 10-11 are the same as 8-9 for templates shifted by  $+0.5$  cycles later the turn-on found. Square brackets  $\square$  indicate that the template phase is rounded to 0.25 or 0.75. For some cycles (e.g. # 253, #254, etc.) we show the template minimization data for different number of template points (the second row in columns 6-7).

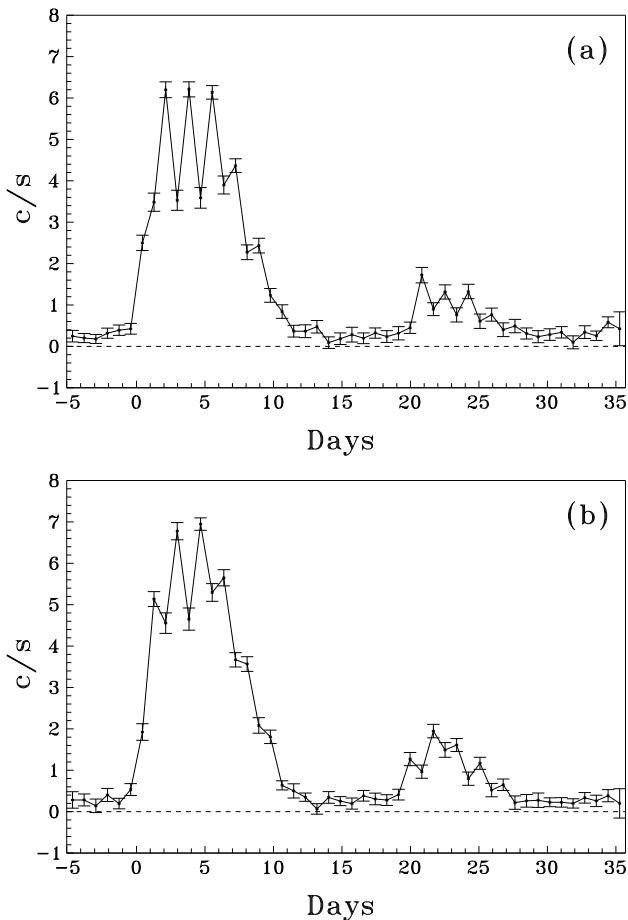
We should shortly comment on Table 1. Practically for all cycles the significance level is found to be  $> 70\%$ . It is interesting to note that although for cycle # 255 the turn-on time is well determined by the signal-to-noise ratio, the use of a long template makes the probability of the cycle's turning-on half an orbit later higher because the form of the X-ray main-on decrease of this cycle is better fitted by 0.75-templates, but we preferred the turn-on time determined by the real data. In addition, nearly for all remaining cycles the probabilities of the turn-on 0.5 orbit before/after the determined value is very small, with the only exception of cycle # 266, for which the probability of turn-on half an orbit earlier is 87%. However, this cycle is poor in data.

As seen from Table 1, the number of cycles with a duration of 20.5 orbits is notably larger than those of 20 or 21 orbits. Moreover, the first nine successive cycles turned on after 20.5 orbits. Clearly, such a distribution is far from being random. There is a small correlation between the duration of a cycle and its mean X-ray flux, those of higher intensity being longer (21 orbits) and of lower intensity shorter (20 orbits). To increase the significance of this correlation a larger number of cycles should be analyzed.

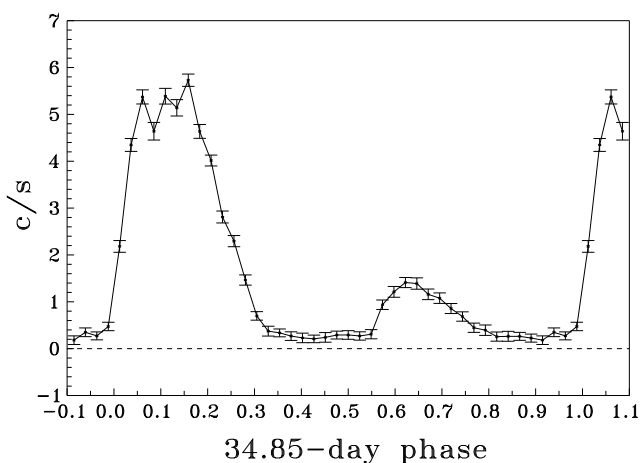
## 2.2 The mean X-ray light curves

Fig. 2(ab) display the mean X-ray light curves constructed by superimposing separately 35-d cycles turned-on near orbital phase 0.25 (Fig. 2a) and 0.75 (Fig. 2b). The points inside the X-ray eclipses, i.e. in orbital phase interval  $0.932 \div 0.068$ , were excluded. In Fig. 2a (0.25-cycles), the zero-point of 34.85-d period corresponds to the phase 0 of the orbital cycle at which the turn-on occurred, while in Fig. 2b (0.75-cycles) it relates to the phase 0.5 of the orbital cycle where the turn-on occurred. As seen from Fig. 2ab, the pre-eclipse X-ray absorption dips are clearly visible on the mean light curves. Moreover, they are also seen in the low-on state.

Fig. 3 shows the mean X-ray light curve obtained by adding the curves from Fig. 2ab, assuming the average duration of each cycle to be exactly 20.5 orbits, for which we have stretched a little the cycles of shorter duration and correspondingly compressed the longer ones. Due to zero-points of the mean 0.25- and 0.75-light curves differing by  $\Delta\Phi_b = 0.5$  by construction, the absorption dips on the resulting total light curve should have been compensated for. Nevertheless, the first pre-eclipse dip on the 0.25-light curve is so strong that it is not compensated for and remains clearly visible on the mean X-ray light curve.



**Figure 2.** The mean RXTE X-ray light curve of Her X-1 for cycles turning-on at  $[\Phi_b = 0.25]$  (a) and at  $[\Phi_b = 0.75]$  (b) obtained by folding the corresponding cycles without changing their actual duration.



**Figure 3.** The mean X-ray light curve of Her X-1 obtained by adding all 0.25 and 0.75-cycles with stretching or compressing the cycles to a standard duration of 20.5 orbits.

In spite of a much smaller statistics, the general shape of the mean RXTE X-ray light curve looks very similar as found from UHURU data (Jones & Forman 1976). Qualitatively, both main-on and short-on stages are visible. During the main-on stage, the source reaches the peak count rate in 1.5 orbits, stays at maximum for 2.5 orbits, and progressively fades to minimum during 3 orbits. The beginning of the short-on stage is separated by 4.5 orbits from the end of the main-on. The duration of the short-on state is about 5 orbits.

Note that the form of the short-on stage is similar to that of the main-on: a rapid increase and slow decrease of count rate. The main-on state is separated by a similar 4.5 orbits' off-state from the end of the short-on state. A slow increase in count rate before the main-on state (first noted by Jones & Forman (1976)) is also clearly seen. A weak X-ray glow persistent during off-states is possibly due to scattering in the accretion disk corona.

### 2.3 Dips and other features

In order to investigate in more detail the form and features of the RXTE X-ray light curve of Her X-1, we folded separately the cycles turning on at binary phases 0.25 and 0.75 and averaged the data over 20 equal bins in one orbital period (Fig. 4 and 5). Note that for these curves we used *all* available data, including X-ray eclipses. The anomalous dip is clearly seen for 0.25-cycles during the first orbit after the main turn-on and is practically invisible for 0.75-cycles. For both types of cycles, the pre-eclipse dips demonstrate the identical behaviour – they march from the eclipse toward earlier orbital phase in successive orbits. In Table 2 we list the orbital phases of ingress to and egress from the pre-eclipse dips (PI, PE) and the anomalous dip (AI, AE). Note also that post-eclipse recovery (RE) is not present in the mean light curves.

Both for 0.25 and 0.75-cycles, the low-on state turns on in the 12th orbit after the main turn-on. After the turn-on, both post-recovery and anomalous dips are present during two successive orbits. In the 15th orbit, the X-ray source emerges immediately after the eclipse and the anomalous dip is absent. In the 16th and 17th cycles, a post-recovery dip may be marginally distinguished for 0.25-cycles. The pre-eclipse dips march likely to the main-on state.

### 3 ACCRETION DISK MODEL CONSTRAINTS

The durations of main-on and short-on states may be used to put bounds on disk geometrical parameters: its inclination to the orbital plane  $\delta$  and the semi-thickness-to-radius ratio  $H/R$ . The disk is assumed to be tilted with respect to the orbital plane and to counter-precess due to tidal interaction with the optical star.

From the duration of the main-on  $d_m$  and low-on  $d_l$  states we can determine the dependence of the disk inclination to the orbital plane  $\delta$  and the parameter  $H/R$ , on the binary inclination  $i$ . The angle between the disk normal and the line of sight  $\theta$  relates with the azimuthal angle of disk precession  $\phi$  as

$$\cos \theta = \cos \delta \cos i + \sin \delta \sin i \cos \phi.$$

This figure is available at URLs:

<http://xray.sai.msu.ru/pub/preprints/Prokhorov/rxte/fig4a.ps>  
or  
<http://xray.sai.msu.ru/pub/preprints/Prokhorov/rxte/fig4a.ps>

This figure is available at URLs:

<http://xray.sai.msu.ru/pub/preprints/Prokhorov/rxte/fig4b.ps>  
or  
<http://xray.sai.msu.ru/pub/preprints/Prokhorov/rxte/fig4b.ps>

**Figure 4.** The mean RXTE light curve of Her X-1 for all 34.85-d cycles that turn on near  $\Phi_b = 0.25$ . The vertical quadrangles mark X-ray eclipses. Points are individual RXTE observations. These points are averaged in 20 bins per one orbit. Bars show the mean count rate plus/minus rms error inside these bins.

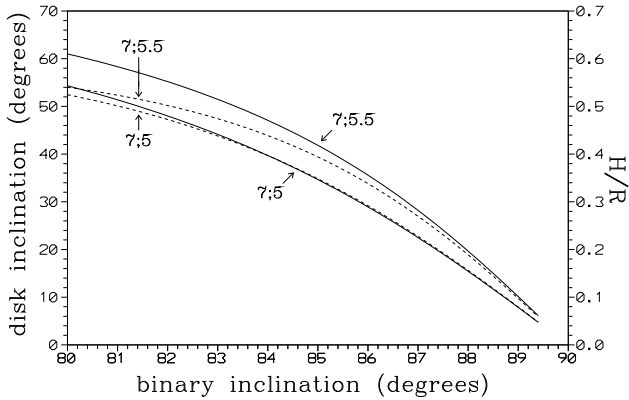


**Figure 6.** The disk inclination angle  $\delta$  (solid lines) and its dimensionless semi-thickness  $H/R$  (dashed lines) as a function of binary inclination angle  $i$ . The lines are labeled with the duration of the main-on (7) and short-on (5 or 5.5) states in orbital periods.

For the main-on state  $\theta = \theta_m \equiv \pi - \arctan(H/R)$ , whereas for the low-on state  $\theta = \theta_l \equiv -\theta_m$ . Using these relations we obtain

$$\delta = -\arctan\left(\frac{2}{\tan i(z_m + z_l)}\right)$$

and

$$H/R = \arcsin\left(\frac{z_m - z_l}{2} \sin \delta \sin i\right),$$

where

$$z_m \equiv \cos(2\pi d_m/P_{prec}), \quad z_l \equiv \cos(2\pi d_s/P_{prec}),$$

and  $P_{prec}$  is the disk precession period. Fig. 6 shows  $\delta$  and  $H/R$  as a function of the orbital inclination  $i$  for limiting durations  $d_m$  and  $d_l$  expressed in orbital cycles.

#### 4 CONCLUSIONS

The analysis of the publically available RXTE data on Her X-1 confirmed main features of 34.85-d cycle of Her X-1. We have determined turn-on times of new RXTE cycles with a good accuracy. The use of template light curves has enabled

us to find turn-on times of the cycles with data gaps near the turn-on. We discovered that the number of cycles with a duration of 20.5 orbits is significantly higher than those of shorter or longer duration, thus casting doubts as to the randomness in the successive cycle durations. Instead, a small correlation between the mean X-ray flux and the cycle duration has been found. Such a correlation has also been noted in BATSE data (Wilson et al. 1994). This correlation is possibly related to the dynamical action of accreting streams on the precessional motion of the accretion disk, with the tidal interaction forcing the disk to counter-precess while the dynamical action pushing the disk into co-orbital precession. The higher accretion rate, the stronger action of streams, hence, the longer the net precessional cycle duration is.

Using the mean X-ray light curve, we have found that the form of the secondary turn-on state looks similar to that of the main-on state, i.e. is characterized by a rapid increase and a slow decrease, with the total duration of 5-5.5 orbital cycles. We also studied the absorption features (dips) and post-recovery on the mean X-ray light curve. We have found that during the main-on state the anomalous dip is present only in one orbit after the turn-on, whereas during low-on state, the anomalous dip is clearly visible during two orbits after the turn-on. The post-eclipse recovery have not been found in main-on state but appears at least two times during low-on state. The pre-eclipsing dips are found in both main-on and low-on states and demonstrate the behaviour as in previous observations.

#### ACKNOWLEDGMENTS

The authors acknowledge the referee, Prof. F.Nagase, for pointing to an inaccuracy in our analysis, and for suggesting the use of templates in the determination of the turn-on times for cycles with data gaps. Research has made use of data obtained through the High Energy Astrophysics Science Archive Research Center Online Service, provided by the NASA/Goddard Space Flight Center. This work is partially supported by the RFBR grant 98-02-16801, by the NTP program "Astronomija" (project 1.4.4.1) of Ministry of Science and High Technology, and by INTAS grant 93-3364-Ext.

This figure is available at URLs:

<http://xray.sai.msu.ru/pub/preprints/Prokhorov/rxte/fig5a.ps>  
or  
<http://xray.sai.msu.ru/pub/preprints/Prokhorov/rxte/fig5a.ps>

This figure is available at URLs:

<http://xray.sai.msu.ru/pub/preprints/Prokhorov/rxte/fig5b.ps>  
or  
<http://xray.sai.msu.ru/pub/preprints/Prokhorov/rxte/fig5b.ps>

**Figure 5.** The same as in Fig. 4 for the cycles turning on near  $\Phi_b = 0.75$ .

## REFERENCES

- Bahcall J.N., Bahcall N.A., 1972, ApJ, 178, L1  
 Baykal A., Boynton P.E., Deeter J.E., Scott D.M., 1993, MNRAS, 265, 347  
 Bildsten L. et al., 1997, ApJSS 113, 367  
 Brecher K., 1972, Nat, 239, 325  
 Cherepashchuk A.M., Efremov Yu. N., Kurochkin N.E., Shakura N.I., Sunyaev R.A., 1972, Inform. Bull. Variable Stars 720  
 Cooke B.A., Page C.G., 1975, Nat, 256, 712  
 Crosa L.M., Boynton P.E., 1980, ApJ, 235, 999  
 Davison P.J.N., Fabian A.C., 1974, MNRAS, 169, 27P  
 Davison P.J.N., Fabian A.C., 1977, MNRAS, 178, 1P  
 Deeter J.E., Boynton P.E., Pravdo S.H., 1981, ApJ, 247, 1003  
 Deeter J.E., Boynton P.E., Miyamoto S., Kitamoto S., Nagase F., Kawai N., 1991, ApJ, 383, 324  
 Fabian A.C., Pringle J.E., Rees M.J., 1973, Nat, 224, 212  
 Gerend D., Boynton P.E., 1976, ApJ, 209, 562  
 Giacconi R., Gursky H., Kellogg E., Levinson R., Schreier E., Tananbaum H., 1973, ApJ, 184, 227  
 Gorecki A. et al., 1982, ApJ, 256, 234  
 Howarth I.D., Wilson B., 1983, MNRAS, 202, 347  
 Jones C.A., Forman W.H., Liller W., 1973, ApJ, 182, L109  
 Jones C., Forman W., 1976, ApJ, 209, L131  
 Levine A.M., Jernigan J.G., 1976, ApJ, 262, 294  
 Liller W., 1972, IAUC, 2415  
 Kurochkin N.E., 1972, Peremennye Zvezdy, 18, 425  
 Mironov A.V., Moshkalev V.G., Trunkovskij E.M., Cherepashchuk A.M., 1984, PAZh, 10, 429  
 Nagase F., Hayakawa S., Kii T. et al., 1984, PASJ, 36, 667  
 Novikov, I.D., 1973, AZh, 50, 459  
 Ögelman H., Kahabka P., Pietsch W., Trümper J., Voges W., 1985, Space Sci. Rev., 40, 347  
 Ögelman H., 1987, A&A, 172, 79  
 Ögelman H., Trümper J., 1988, in Pallavicini R., White N.E., eds., X-ray Astronomy with EXOSAT, Mem. S.A.It., 59, 169  
 Ohashi D., Inoue H., Kawai N., Koyama K., Matsuoka M., Mitani K., Tanaka Y., 1984, PASJ, 36, 719  
 Ricketts M.J., Stanger V., Page C.G., 1982, in Brinkmann W., Trümper J., eds, Accreting Neutron Stars, ISO (Garching bei München), 100  
 Shakura N.I., Postnov K.A., Prokhorov M.E., 1998, A&A, 331, L37  
 Sheffer E.K., Kopaeva I.F., Averintsev M.B. et al., 1992, AZh, 69, 82  
 Shklovskii I.S., 1973, AZh, 50, 233  
 Soong Y., Gruber D.E., Rothschild R.E., 1987, ApJ, 319, L77  
 Staubert R., Bezler M., Kendziorra E., 1983, A&A, 117, 215  
 Tananbaum H., Gursky H., Kellogg E.M., Levinson R., Schreier E., Giacconi R., 1972, ApJ, 174, L143  
 Trümper J., Kahabka P., Ögelman H., Pietsch E., Voges W., 1986, ApJ, 300, L63  
 Von Wentzel W., Gessner H., 1972, Mitt. Ver. Sterne, 6, 61  
 Wilson R.B., Finger M.H., Pendelton G.N., Briggs M., Bildsten L., 1994, in Holt S.S., Day C.S., eds, The Evolution of X-ray Binaries, AIP Press (New York), 475

**Table 2.** Dips on the mean 0.25 and 0.75 X-ray light curves.

Orb. cycle	Orb. phase	Error	Type	Orb. phase	Error	Type
	0.25			0.75		
Main-on						
1	0.500	0.025	AI	...	...	...
	0.575	0.025	AM	...	...	...
	0.663	0.013	AE	...	...	...
	0.813	0.013	PI	...	...	...
	...	...	...	0.838	0.013	PI
2	0.788	0.013	PI	...	...	...
	...	...	...	0.813	0.013	PI
3	0.725	0.025	PI	...	...	...
	...	...	...	0.788	0.013	PI
	0.913	0.013	PBE	0.913	0.013	PBE
4	0.713	0.013	PI	...	...	...
	...	...	...	0.738	0.013	PI
	0.850	0.025	PBE	...	...	...
	...	...	...	0.888	0.013	PBE
5	0.675	0.038	PI	...	...	...
	...	...	...	0.713	0.013	PI
	0.825	0.038	PBE	...	...	...
	...	...	...	0.850	0.025	PBE
6	0.650	0.038	PI	0.650	0.025	PI
	0.750	0.038	PBE	...	...	...
Low-on						
12	0.25:	...	TO	0.25:	...	TO
13	0.17	0.025	RE	...	...	...
	...	...	...	0.20	0.05	RE
	0.45	0.05	AI	...	...	...
	...	...	...	0.50	0.05	AI
	0.65	0.05	AE	0.65	0.05	AE
	0.75	0.05	PI	0.75	0.05	PI
14	0.20	0.05	RE	0.20	0.05	RE
	0.45	0.05	AI	...	...	...
	0.60	0.05	AE	...	...	...
	0.70	0.05	PI	0.70	0.05	PI
15	0.65	0.05	PI	0.65	0.05	PI
16	0.20:	...	RE	...	...	...
	0.70:	...	PI	...	...	...
	0.85:	...	PE	...	...	...
17	0.20:	...	RE	...	...	...

TO – turn-on time; AI, AM, AE – ingress to, minimum of, and egress from the anomalous dip; PI, PBE – ingress to and the beginning of egress from the pre-eclipse dip; RE – post-eclipse recovery.